Understanding Magnetic Interaction Pathways: An Experimental Determination of Electron Density in an Alkyne-Substituted Nitronyl Nitroxide Radical

Nicolas Claiser,[†] Mohamed Souhassou,*[,†] Claude Lecomte,[†] Yves Pontillon,[‡] Francisco Romero,[§] and Raymond Ziessel[||]

LCM3B, CNRS UMR 7036, Faculté des Sciences, Université Henri Poincaré Nancy I, BP 239, 54506 Vandoeuvre-lès-Nancy, France, CEA/DEN/DEC/S3C, Cen-Cadarache, 13108 Saint Paul-les-Durance, France, Departament de Química Inorgànica, Universitat de València, Dr. Moliner, 50 E, 46100 Burjassot (València), Spain, and LCEPM associé au CNRS ESA-7008, Ecole Européenne de Chimie, Polymères et Matériaux (ECPM), 25 rue Becquerel, BP 08, 67087 Strasbourg Cedex, France

Received: September 17, 2002

In order to understand magnetic interaction pathways, an experimental electron density distribution was determined in a purely organic free radical, *m*-(ethynyl)pyridyl nitronyl nitroxide, using accurate X-ray diffraction measurements. The intermolecular contacts were characterized by a topological analysis of the experimental electron density. Hydrogen bonds involving the O−N−C−N−O fragment reveal a 3D character. Atomic charges obtained by integration over the topological atomic basins indicate a charge transfer from the two oxygen atoms to the C≡C triple bond by electron conjugation through the molecular skeleton, but also possibly through a short hydrogen bond. The X-ray results are compared to theoretical DFT calculations and to experimental spin densities obtained by polarized neutron diffraction.

Introduction

An attractive challenge facing the field of material science concerns the search for novel spin systems displaying valuable physical properties such as ferro- or ferrimagnetism.[1−3] Along these lines, the search for purely organic magnets is a subject of intense research activities.[4] The first genuine example of such a compound is the β-phase of the *p*-nitrophenyl nitronyl nitroxide derivative (*p*-NPNN),[5] for which the magnetic properties are associated with a delocalized unpaired p electron ($S = 1/2$). Furthermore, these stable nitronyl nitroxide (NN) radicals can be used as building blocks, either by themselves (all organic),[6] or in conjunction with transition metal salts.[7] Interestingly, when ionic nitronyl nitroxide radicals are engineered they could be used as a templating frame in the formation of extended inorganic networks.[8] The nitronyl nitroxide radicals exhibit various magnetic behavior (from paramagnetism to ferro- or antiferromagnetism),[9−16] depending on the crystal packing and the chemical composition. By tailoring the organic shell of the molecule, the overlap of particular orbitals with neighboring molecules could be significantly perturbed, and favorable ferromagnetic interactions of the spins could be observed. In light of previous studies, using different techniques (EPR, μSR, ...), it appears that weak intermolecular interactions play a crucial role in the emergence of ferromagnetic interactions between the spins across the multidimensional network. The magnetic behavior can be sometimes predicted using McConnell[17,18] or Kahn and Briat[19] models. However, in recent studies, a geometrical approach based on crystal packing for a large number of nitroxide compounds did not show any systematic correlation between the magnetic behavior and the three-dimensional crystal packing.[20,21] With the aim of studying these intermolecular interactions, we decided to undertake an experimental determination of the electron density using high-resolution X-ray diffraction on a NN radical bearing an ethynyl function as crystal director and a pyridine core labeled HC≡CPyNN (Figure 1) which displays ferromagnetic interactions at cryogenic temperature with an antiferromagnetic order at $T_N = 0.54$ K.[22] Combined with spin density, obtained by polarized neutron diffraction, the electron density and its topological analysis are useful tools to investigate intra- and intermolecular interactions. Polarized neutron measurements[23] and theoretical calculations[24] are available and will serve for comparison purposes with our previous study on similar NN radicals constructed around a thiomethylphenyl framework (NNPhSMe).[25]

Materials and Methods

For X-ray measurements, a black single crystal of dimensions $0.44 \times 0.50 \times 0.48$ mm^3 was mounted on a Nonius Kappa-CCD diffractometer and diffraction data were measured using graphite monochromatized Mo Kα radiation ($\lambda = 0.71073$ Å). The relatively large size of the sample is justified by the low diffracting power of the crystal. The crystal was cooled to 110 K using a N_2 Oxford cryosystem-cooling device. Data up to a resolution of $(\sin\theta)/\lambda = 1.14$ Å^{-1} were collected using two different oscillation widths. First, 1080 images (oscillation width = 1.5°) and second, 655 images (oscillation width = 2.0°) were measured. For each set, exposure time per degree and detector-to-crystal distance were kept fixed and the collection strategy was quite similar for the two sets. The final cell parameters were obtained at the end of the overall data collection by refinement against all the collected reflections (155483). More details about the experimental settings and crystal data are reported in Table 1. Reflections were integrated using the program DENZO[26] implemented in the HKL 2000 package.[26]

* Corresponding authors. E-mail: souhasso@lcm3b.u-nancy.fr
[†] Université Henri Poincaré Nancy I.
[‡] Cen-Cadarache.
[§] Universitat de València.
[||] Ecole Européenne de Chimie, Polymères et Matériaux.

10.1021/jp0270093 CCC: $22.00
Published on Web 11/22/2002

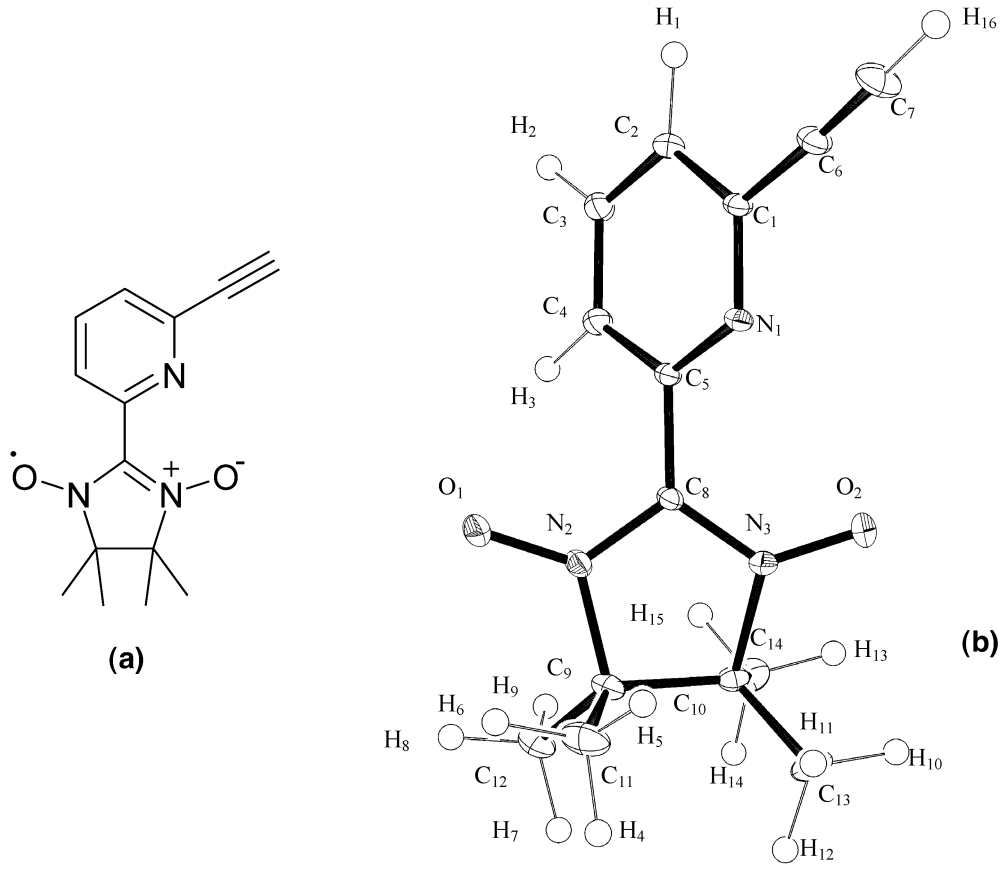

Figure 1. (a) Chemical structure of one mesomeric form and (b) ORTEP[33] view of HC≡CPyNN radical. Thermal ellipsoids are plotted at the 50% probability level.

TABLE 1: Experimental and Crystallographic Details

chemical formula	$O_2N_3C_{14}H_{16}$
space group, cell setting	$P2_1/n$, monoclinic
a, b, c (Å)	6.3075(1), 11.8918(2), 17.5961(2)
β (°), V (Å^3), Z	93.556(1), 1317.3(1), 4
μ (mm^{-1}), D_x calculated (g/cm^3)	0.084, 1.303
X-ray Data Collection (Nonius Kappa CCD)	
T (K), wavelength (Å)	110, 0.71074 Mo(Kα)
scan method, oscillation width (°)	φ and ω rotations, 1.5 and 2.0
exposure time per degree (s)	120
crystal to detector distance (mm)	40
no. of frames, no. of measured reflections	1735, 155483
range of h,k,l, $(\sin\theta/\lambda)_{max}$ (Å^{-1})	$-9 < h < 9$, $-27 < k < 25$, $-40 < l < 37$, 1.14
no. of independent reflections	14931
R_{int}[a] (%), overall completeness (%)	5.75, 91.2
Neutron Data Collection (ILL, D9, Grenoble) and Refinement	
T (K), wavelength (Å)	110, 0.8398
a, b, c (Å); β (°)	6.3130(4), 11.8844(7), 17.5828(10); 93.537(5)
no. of measured and independent reflections	3340, 2557
no. of significant reflections: $F_o > 4\sigma(F_o)$	2283
range of h,k,l, $(\sin\theta/\lambda)_{max}$ (Å^{-1})	$-8 < h < 1$, $-16 < k < 9$, $-23 < l < 23$, 0.68
R_{int}[b] (%), R_σ[c] (%)	2.55, 4.38
R_1[e]	5.24 for 2283 $F_o > 4\sigma(F_o)$; 6.30 for 2557 uniques
wR_2,[d] GOF[f]	11.49, 0.949

[a] $R_{int} = [\sum_H \sqrt{(N/N-1)} \sum_{i=1}^{N_{equiv}} |I_i - \langle I \rangle|] / [\sum_H \sum_i |I_i|]$. [b] $R_{int} = [\sum |F^2_{obs} - \langle F^2_{obs} \rangle|] / [\sum F^2_{obs}]$. [c] $R_\sigma = [\sum \sigma(F^2_{obs})] / [\sum F^2_{obs}]$. [d] $wR_2 = \{[\sum w(F^2_{obs} - F^2_{calc})^2] / [\sum w(F^2_{obs})^2]\}^{1/2}$. [e] $R_1 = [\sum ||F_{obs}| - |F_{calc}||] / [\sum |F_{obs}|]$. [f] $GOF = \{[\sum w(F^2_{obs} - F^2_{calc})^2] / [n - p]\}^{1/2}$.

Then, the data were corrected from absorption effects using the ABSORB[27] program and finally sorted, scaled, and averaged using SORTAV.[28] The crystal did not present any decay during the data collection as checked by the evolution of the interframe scale factors versus time. The linear absorption coefficient $\mu_{Mo-K\alpha} = 0.0837$ mm^{-1} leads to maximum and minimum transmission factors of 0.982 and 0.970. The 155483 observed reflections were merged into 14931 independent reflections with

TABLE 2: X-ray Data Internal Agreement Indices versus Resolution (no sigma cutoff)

$S = \sin\theta/\lambda$ (Å^{-1})	N_{terms}	N_{mean}	R_1[a]	R_2[b]	R_w[c]
$S < 0.42$	17595	788	0.0422	0.0510	0.1140
$0.42 < S < 0.53$	20013	827	0.0488	0.0572	0.0631
$0.53 < S < 0.61$	16204	809	0.0594	0.0711	0.0743
$0.61 < S < 0.67$	14205	806	0.0640	0.0754	0.0786
$0.67 < S < 0.72$	13095	807	0.0728	0.0813	0.0891
$0.72 < S < 0.76$	10646	813	0.0815	0.0887	0.0978
$0.76 < S < 0.80$	9516	768	0.1007	0.1044	0.1169
$0.80 < S < 0.84$	8378	793	0.1116	0.1153	0.1269
$0.84 < S < 0.87$	7363	741	0.1174	0.1205	0.1325
$0.87 < S < 0.91$	7054	760	0.1387	0.1363	0.1539
$0.91 < S < 0.93$	5485	702	0.1657	0.1519	0.1718
$0.93 < S < 0.96$	5267	696	0.1930	0.1801	0.1949
$0.96 < S < 0.99$	4855	699	0.2049	0.1950	0.2021
$0.99 < S < 1.01$	3406	626	0.2003	0.1751	0.2023
$1.01 < S < 1.04$	2952	591	0.2307	0.2061	0.2230
$1.04 < S < 1.06$	2795	591	0.2464	0.2725	0.2671
$1.06 < S < 1.08$	2157	529	0.2558	0.2350	0.2506
$1.08 < S < 1.10$	1197	420	0.2840	0.2723	0.2842
$1.10 < S < 1.12$	1016	367	0.2889	0.2694	0.2965
$1.12 < S < 1.14$	786	300	0.3314	0.3020	0.3291
total	153985	13433	0.0575	0.0564	0.0966

[a] $R_1 = [\sum_H\sqrt{(N/N-1)}\sum_{i=1}^{N_{equiv}}|I_i - \langle I\rangle|]/[\sum_H\sum_i|I_i|]$. [b] $R_2 = \{[\sum_H\sqrt{(N/N-1)}\sum_{i=1}^{N_{equiv}}(I_i - \langle I\rangle)^2]/[\sum_H\sum_i(I_i)^2]\}^{1/2}$. [c] $R_w = \{[\sum_H\sqrt{(N/N-1)} \times \sum_{i=1}^{N_{equiv}} w[(I_i - \langle I\rangle)/\sigma(I_i)]^2]/[\sum_H\sum_i w[I_i/\sigma(I_i)]^2]\}^{1/2}$, where w is the weighting scheme[28] ($w_{(I)} = \sigma_{(I)}^{-2}$).

an overall completeness of 91.2% up to the maximum resolution of 1.14 Å^{-1}. This data collection strategy enabled a high redundancy (10.4 on average), improving the precision of the intensities that is required for an accurate crystallographic study. It is important to point out the very good internal agreement indice for the whole data set ($R_1 = 5.75\%$ without any σ cutoff; Table 2); it however shows large values for high-resolution data. This observation underlines the experimental difficulties for obtaining accurate high-resolution data with a Nonius Kappa CCD diffractometer.

To have precise hydrogen atomic positions and thermal parameters, an unpolarized neutron diffraction experiment was carried out in parallel at the Institut Laue-Langevin (ILL) at Grenoble on the D9 four-circles diffractometer. A single crystal in the form of a regular slab (dimension of $3 \times 2 \times 1$ mm^3) was cooled to 110 K, using an Air Products Displex cryostat cooling device, at the same temperature as the X-ray experimental temperature. In a first step, the orientation matrix together with cell parameters were determined and refined by a least-squares procedure on 20 independent reflections. Then final cell parameters were refined on 657 strong reflections ($5.47° < \theta < 34.64°$) after data collection (Table 1); 3340 reflections were collected up to $\sin\theta/\lambda = 0.68$ Å^{-1}. The RACER[29] program was used to calculate all of the integrated intensities. The absorption coefficient $\mu = 0.1898$ mm^{-1} was determined assuming $\sigma = 38$ barn for hydrogen atoms and then used to calculate the absorption correction by estimating the mean path in the crystal for each (hkl) reflection collected ($0.168 \le (I - I_0)/I_0 \le 0.224$). Complete crystal data and experimental parameters at $T = 110$ K are displayed in Table 1.

Structure Determination. In a preliminary step, the crystal structure was redetermined using the SHELX package[30,31] and refined using MOLLY[32] against neutron diffraction data. This process led to the final agreement indices $R = 6.23\%$, $R_w = 3.72\%$, GOF = 2.04 for 2557 reflections and 316 parameters. Then, using the structure obtained from the neutron experiment as starting model, the structure was refined with SHELXL97[31] against X-ray diffraction data. The thermal displacement parameters, isotropic for hydrogen atoms and anisotropic for all non-hydrogen atoms, were refined using F^2 ($R_1 = 5.41\%$, $wR_2 = 13.37\%$, GOF = 0.84 for 8659 reflections with $I > 4\sigma$ and 236 parameters). The chemical representation of the molecule and the ORTEP[33] view are shown in Figure 1.

Multipolar Refinements. To model accurately the electron density distribution, a multipolar model as defined in MOLLY[32] was used (eq 1):

$$\rho(\vec{r}) = \rho_{core}(r) + P_v\kappa^3\rho_v(\kappa r) + \sum_{l=0}^{l_{max}}\kappa'^3 R_l(\kappa' r)\sum_{m=0}^{+1}\sum_p P_{lmp}y_{lmp}(\theta,\varphi) \quad (1)$$

with

$$R_l(r) = \frac{\zeta_l^{n_l+3}}{(n_l+2)!}\, r^{n_l}\, e^{-\zeta_l r} \quad (2)$$

The first two terms $\rho_{core}(r)$ and $\rho_v(r)$ are respectively the spherically averaged core and valence electron densities of the free atom, calculated from Clementi and Raimondi wave functions.[34] The last term is the expansion of the valence density on the spherical harmonic functions in real form y_{lmp} which take into account the deformation of the density due to the chemical bonding. P_v is the valence electron populations, P_{lmp} are the multipole populations, and κ, κ' are contraction expansion parameters. The radial functions $R_{nl}(r)$ were chosen as Slater type (eq 2). For all non-hydrogen atoms, the initial n_l values are 2−2−3−4 ($l_{max} = 3$) and the ζ_l parameter was 3.0 Bohr^{-1} (single-ζ) for O and C atoms, 3.8 Bohr^{-1} for N atoms. Due to the particular shape of the electron density on the NN function, for oxygen, nitroxide nitrogens (N_2 and N_3), and C_8 atoms, l_{max} was taken equal to 4. For H atoms, the n_l and ζ_l were 0−1 and 2.26 Bohr^{-1}, respectively ($l_{max} = 1$). The contracted form factor of the hydrogen atom ($\kappa = 1.16$) was used.[35] The anomalous dispersion coefficients were those of Cromer.[36] An electroneutrality constraint was applied during the refinements.

To analyze the modeled electron density, one can inspect two different density maps. First, the residual density (eq 3), which

is the difference between modeled and observed electron densities, allows to judge the quality of the refinement:

$$\Delta\rho_{\mathrm{resi}}(\vec{r}) = \frac{1}{V}\sum_{\vec{H}}\left(\frac{1}{k}\left|F_{\mathrm{obs}}(\vec{H})\right| - \left|F_{\mathrm{calc}}(\vec{H})\right|\right) e^{i\Phi_{\mathrm{calc}}} e^{-2i\pi\vec{H}\cdot\vec{r}} \quad (3)$$

where F_{obs} and F_{calc} are the structure factor amplitudes observed and calculated using the multipolar atom model, k is the scale factor, V is the cell volume, $\vec{H}$ is a vector in the reciprocal space and Φ_{calc} is the structure factor phase calculated from the multipolar model.

Static deformation density maps (eq 4) are also shown, defined as the difference between the modeled static total electron density (eq 1) and the sum of spherical averaged independent atom densities (IAM model):

$$\Delta\rho(\vec{r}) = P_v\kappa^3\rho_v(\kappa r) - N_v\rho_v(r) + \sum_{l=0}^{l_{\max}}\kappa'^3 R_l(\kappa' r)\sum_{m=0}^{+1}\sum_{p} P_{lmp} y_{lmp}(\theta,\varphi) \quad (4)$$

where N_v is the number of valence electrons of the free atom. In this paper, these maps were calculated and plotted in the pyridine and nitronyl ring planes.

Topology of the Electron Density. The total electron density can be analyzed in a quantitative way using the theory "Atoms In Molecules, A Quantum Theory" developed by Bader.[37] From the spatial distribution of the electron density, one can derive the gradient trajectories ($\vec{\nabla}\rho$), the Laplacian distribution ($\nabla^2\rho$), and the location of all critical points (CP), i.e. where the gradient of ρ vanishes, and the associated topological features. The nature of the CP is determined by the eigenvalues (curvatures) of the Hessian matrix ($\partial^2\rho(r)/\partial x_i\partial x_j$). This topological analysis permits partitioning of the total electron density into atomic basins, and volume integration carried out on these basins gives access to the net atomic charges.

A new version of the program NEWPROP[38] was used to locate the CP and to calculate the topological properties and integrated charges of the modeled electron density. The uncertainties on the topological properties are not rigorously calculated, but an estimation of the uncertainties on the position of the CP is in the order of 0.001 Å, and the uncertainty of the laplacian calculated using the covariance matrix is about 10%. So, the errors we estimate are $\sigma(\rho) \approx 0.01$ eÅ^{-3}, 0.001 Å for the CP atom distances, and 10% for the curvatures ($\Delta\lambda/\lambda$). An example of gradient trajectories in the pyridine ring plane (a) and of the Laplacian of the total electron density in the nitronyl ring (b) are given in Supporting Information (Figure S1).

Results: Multipolar Refinement of HC≡CPyNN

Our first aim was to use the neutron determined positional and thermal parameters, which are unbiased by valence density distribution. Unfortunately, due to large discrepancies of neutron and X-ray atomic displacement parameters (ADP), positions and U_{ij} of non-H atoms were first refined against high order (HO) X-ray reflections using the Independent Atom Model (IAM, Table 3). All hydrogen atom parameters were then refined against low order (LO) reflections, which led to an average C−H distance of 1.04(2) Å ($R = 5.08\%$, $R_w = 5.77\%$, GOF = 1.20). To avoid biases in the electron density modeling due to the shift of the electron density distribution toward the atom linked to H, each carbon−hydrogen distance was then adjusted to the value obtained from our neutron diffraction experiment (average C−H distance of 1.089(5) Å). During the multipolar refinement, a unique set of κ, κ' was used for each of the following groups: (C_1, C_5, C_8), (C_2, C_3, C_4), (C_6, C_7), (C_9, C_{10}), (C_{11}, C_{12}, C_{13}, C_{14}), (N_2, N_3), and (O_1, O_2) (see Figure 1). All hydrogen atoms were constrained to have the same κ value.[39] Due to large uncertainties on HO structure factor modulii [$(\sin\theta)/\lambda > 0.9$ Å^{-1}] after the $P_v-\kappa$ refinement,[40] a full multipolar refinement using only reflections with intensities greater than 3σ and $(\sin\theta)/\lambda < 0.9$ Å^{-1} was performed ($N_{\mathrm{ref}} = 5731$). The agreement indices at the end of the full multipolar model refinement are excellent ($R = 1.60\%$, $R_w = 2.10\%$, and GOF = 0.53), attesting for the quality of the data used for the refinement.

The average estimated standard deviation of the electron density as defined in (eq 5),

$$\sigma(\rho) = \frac{\sqrt{\sum_{\vec{H}}(\Delta F(\vec{H}))^2}}{V} \quad (5)$$

where $\Delta F(\vec{H})$ is the difference between observed and calculated structure factors, is $\sigma_{(\rho)} = 0.06$ eÅ^{-3}. The quality of our multipolar model is assessed by inspecting the residual density maps (Figure 2). Except for the triple C_6-C_7 and the N_2-O_1 bonds for which the modeled density seems slightly underestimated, a randomly distributed residual density is observed both in the pyridine ring plane (Figure 2a) and in the plane of the nitronyl ring (Figure 2b). It is worth noting that modeling the density of (N−O)$^\bullet$ was difficult, a difficulty we had earlier faced for the analysis of NNPhSMe.[25] Nevertheless, the modeling left to maximum residues of 0.10 eÅ^{-3}.

Table 3 summarizes the refinement indices obtained for all refinements. Atomic positions and ADPs at the end of the multipolar refinement are given as Supporting Information, and interatomic distances and angles are given in Table 4.

Discussion

Structural Analysis. The HC≡CPyNN structure has been previously described at room temperature (X-ray data)[22] and at 6.5 K (neutron data).[24] The chemical structure and the labeling scheme are summarized in Figure 1.

The pyridine ring bond distances are in close agreement with those of similar compounds and the average length ($\langle d\rangle$ = 1.351(7) Å) of the two C_8-N short bonds is in keeping with literature data.[46−51] On the other hand, as expected, the average (N−O)$^\bullet$ distance in HC≡CPyNN ($\langle d\rangle$ = 1.277(9) Å) is significantly higher than the corresponding bonds observed in nitro (NO_2) compounds by Kubicki et al.[46] ($\langle d\rangle = 1.232(6)$ Å), Bianchi et al.[48] ($\langle d\rangle = 1.233(10)$ Å) or Zhurova and Pinkerton[51] ($\langle d\rangle$ = 1.227(2) Å). Hence, an important characteristic of the HC≡CPyNN is the peculiar electronic structure of the nitronyl nitroxide function, which possesses one electron in a π^* molecular orbital delocalized over five atoms (O_1, N_2, C_8, N_3, and O_2). The bond length differences between the N−O of the nitronyl nitroxide radicals and the NO_2 groups[46,48,51] are attributed to the unpaired antibonding electron as confirmed by the PND experiment[23] and theoretical calculations.[24] As generally observed, the unpaired electron contributes to an increase of the N−O bond distances and consequently to a decrease of the electron density at the CP (see below), whereas in case of the molecules described in references 46, 48, and 51, the N−O bond π character is increased by the equilibrium between two mesomeric forms, which contributes to a shortening of the N−O distances.

TABLE 3: Agreement Indices for the Different Refined Models

refinement type[a]	sin θ/λ (Å^{-1})	I/σ	R (%)[b]	R_w (%)[c]	GOF[d]	N_{obs}	N_{var}
IAM	all data	all data	7.89	6.57	1.04	14928	236
	<0.9	>3	3.57	5.28	1.31	5731	236
IAM HO	>0.9	all data	16.83	11.90	0.73	6970	171
	>0.9	>3	4.68	5.73	0.69	1677	171
IAM LO	<0.9	all data	5.08	5.77	1.20	7958	64
multipolar model	all data	all data	6.43	4.61	0.72	14928	349
	<0.9	>3	1.60	2.10	0.53	5731	349

[a] IAM, HO and LO: independent atoms model, high and low order, respectively. [b] $R = [\sum_{\vec{H}}|(1/k)|F_{obs}(\vec{H})| - |F_{calc}(\vec{H})|]/[\sum_{\vec{H}}(1/k)|F_{obs}(\vec{H})|]$. [c] $R_w = \{[\sum_{\vec{H}} w[(1/k)|F_{obs}(\vec{H})| - |F_{calc}(\vec{H})|]^2]/[\sum_{\vec{H}}(1/k^2)w|F_{obs}(\vec{H})|^2]\}^{1/2}$. [d] GOF $= \{[\sum_{\vec{H}} w[(1/k)|F_{obs}(\vec{H})| - |F_{calc}(\vec{H})|]^2]/[N_{obs} - N_{var}]\}^{1/2}$, where $w = \sigma^{-2}(F)$.

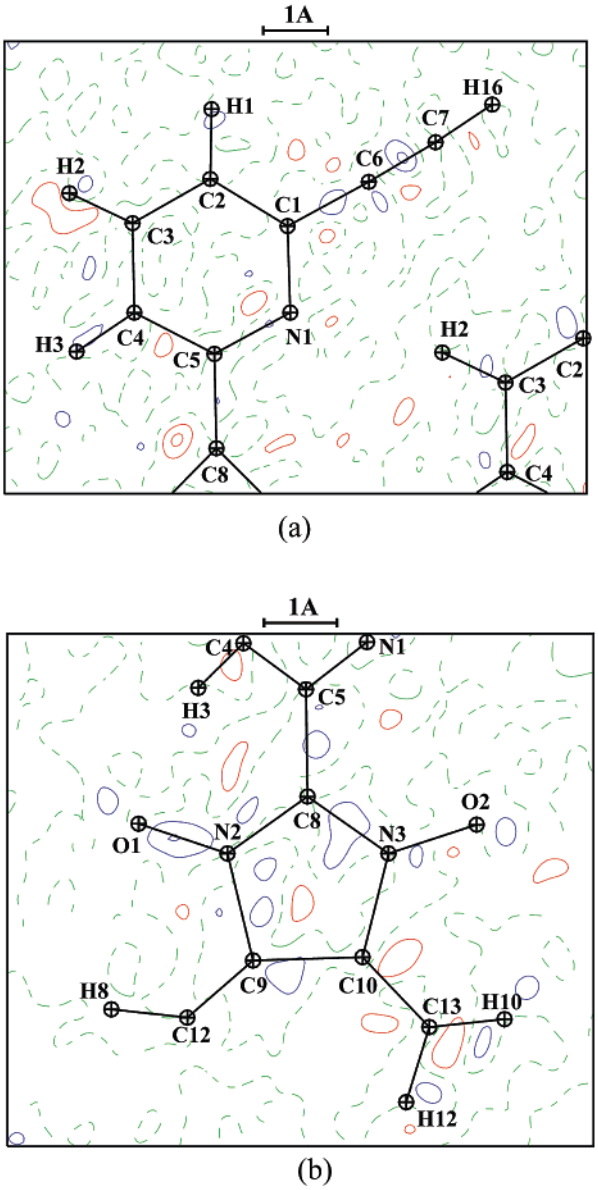

Figure 2. Residual density in (a) the pyridine ring and (b) the nitronyl ring planes [$I > 3\sigma(I)$, $\sin\theta/\lambda < 0.9$ Å^{-1}]. Contours of 0.05 eÅ^{-3} (positive contours in solid lines (red), negative contours in short dashed lines (blue), and long dashed lines for zero contour).

Crystal Packing. The shortest intermolecular contacts of the crystal packing are indicated in Figure 3, selected intermolecular distances and angles are given in Table 4. As also observed in another study (ITPyC≡CH imino-nitroxide radical),[52] the packing can be described as centrosymmetric dimers due to $\pi-\pi$ interaction between ethynyl-pyridine groups in the $(\vec{b},\vec{c})$ plane (Figure 3a). These dimers aggregate in infinite zigzag chains linked by a short hydrogen bond between one nitroxide oxygen atom and the terminal alkynyl hydrogen atom ($d_{O1\cdots H16}$ = 2.132(6) Å). This C−H···O interaction has been exhaustively described in previous studies.[22−24] The ring-stacking distances observed at room temperature, 3.540 Å for ITPyC≡CH and 3.615 Å for HC≡CPyNN are characteristic of such an interaction.[53] In the latter compound, an additional hydrogen bond increases the dimer's stability: $O_2\cdots H_1$ ($d_{O2\cdots H1}$ = 2.309(5) Å). Other intermolecular contacts exist in this plane: $N_1\cdots H_{12}$ ($d_{N1\cdots H12}$ = 2.822(6) Å) and $N_1\cdots H_{14}$ ($d_{N1\cdots H14}$ = 2.519(6) Å) (Figure 3a). A short intermolecular distance is also found between two methyl hydrogen atoms: H_5 and H_{13} ($d_{H5\cdots H13}$ = 2.152(8) Å) corresponding to a van der Waals contact. Finally, the N_2-O_1 and N_3-O_2 groups of adjacent molecules are nearly perpendicular with a distance of 4.2655(3) Å between O_1 and O_2.

In the $\vec{a}$ direction, the nitronyl rings are stacked parallel to each other, whereas the neighboring pyridine rings are coplanar, allowing three weak hydrogen bonds (Figure 3b): O_2 and N_1 exhibit intermolecular contacts with the closest hydrogen atoms of the pyridine ring with $d_{O2\cdots H3}$ = 2.457(5) Å and $d_{N1\cdots H2}$ = 2.493(5) Å (Figure 3b), a third contact involves a methyl hydrogen atom: ($d_{O1\cdots H11}$ = 2.499(6) Å).

Temperature Effects. The cell parameters decrease from room temperature to 110 K by 0.55, 1.59, and 0.32 % for *a*, *b*, and *c*, respectively, and by 1.03, 2.24, and 0.65% from room temperature to 6.5 K (Table 4a). From room temperature to 110 K the general behavior is an increase of most covalent bond lengths. The largest variation is for the triple C_6-C_7 bond (+0.037(3) Å, +3.07%) followed by the bonds of the pyridine ring and C_8-N (Table 4a). The C_6-C_7 triple bond length observed at 110 K is significantly longer than the average value obtained from the Cambridge Crystallographic Data Centre[54] (CCDC) for similar bonds at room temperature [$\langle d_{C\equiv C}\rangle$ = 1.173(9) Å compared to d_{C6-C7} = 1.2061(3) Å in this study], as confirmed by the neutron experiment at 110 K [d_{C6-C7} = 1.206(3) Å]. Similarly, the temperature effect is also important on the intermolecular interactions, leading to a decrease in cell volume at low temperature: all intermolecular contacts decrease, particularly $O_1\cdots C_{13}$ [−0.083(3) Å, −2.32%] and $O_1\cdots O_2$ [−0.082(2) Å, −1.77%]. However, the differences between 110 K and 6.5 K are much smaller. The largest variations concern $O_1\cdots C_{13}$ and $O_1\cdots O_2$ intermolecular bonds [−0.026(7) Å, −0.73% and −0.027(9) Å, −0.58%, respectively]. These observations indicate that π-electron delocalization over the ethynyl-pyridine and NN groups decreases with decreasing temperature, the larger effect being on the triple bond and, correspondingly, the intermolecular interactions become stronger. This can be understood as a polymorphic structural modification that will lead to the magnetic properties observed

TABLE 4a: Cell Parameters and Selected Bond Lengths[a] (Å) at Different Temperatures

	X-ray (298 K)[22]	X-ray (110 K)	neutron (6.5 K)[24]
a (Å)	6.348(1)	6.3075(1)	6.28(2)
b (Å)	12.076(3)	11.8918(2)	11.81(3)
c (Å)	17.640(5)	17.5961(2)	17.53(4)
β (°)	92.94(2)	93.556(1)	93.7(1)
N2−O1	1.285(2)	1.2839(3)	1.277(4)
N3−O2	1.271(2)	1.2708(3)	1.265(4)
N2−C8	1.335(2)	1.3466(3)	1.343(4)
N3−C8	1.348(2)	1.3559(3)	1.363(4)
N2−C9	1.507(3)	1.5091(3)	1.502(4)
N3−C10	1.509(2)	1.5058(3)	1.499(4)
C9−C11	1.530(3)	1.5325(4)	1.540(4)
C9−C12	1.517(3)	1.5217(4)	1.522(5)
C9−C10	1.547(3)	1.5554(3)	1.547(4)
C10−C13	1.515(3)	1.5212(4)	1.521(5)
C10−C14	1.520(3)	1.5299(4)	1.530(5)
C8−C5	1.474(2)	1.4706(3)	1.468(4)
C1−C2	1.391(3)	1.4052(3)	1.402(5)
C2−C3	1.373(3)	1.3886(3)	1.385(5)
C3−C4	1.375(3)	1.3914(3)	1.386(5)
C4−C5	1.378(3)	1.3978(3)	1.393(5)
C5−N1	1.342(2)	1.3404(3)	1.339(4)
C1−N1	1.346(2)	1.3467(3)	1.347(4)
C1−C6	1.445(3)	1.4380(3)	1.434(5)
C6−C7	1.169(3)	1.2061(3)	1.209(5)
C2−H1		1.082(5)	1.073(8)
C3−H2		1.086(5)	1.096(6)
C4−H3		1.081(5)	1.081(7)
C11−H4		1.091(6)	1.077(7)
C11−H5		1.105(6)	1.096(7)
C11−H6		1.097(6)	1.072(8)
C12−H7		1.102(6)	1.080(7)
C12−H8		1.089(5)	1.086(8)
C12−H9		1.081(5)	1.091(7)
C13−H10		1.093(5)	1.067(7)
C13−H11		1.084(6)	1.101(7)
C13−H12		1.093(5)	1.101(8)
C14−H13		1.097(5)	1.095(8)
C14−H14		1.095(5)	1.086(8)
C14−H15		1.094(5)	1.091(7)
C7−H16		1.060(5)	1.053(8)
O2···H1^{iii}	2.443	2.309(5)	2.298(9)
O2···C2^{iii}	3.146(2)	3.1112(2)	3.097(9)
O2···H3^{i}	2.590	2.457(5)	2.415(7)
O2···C4^{i}	3.258(3)	3.1795(3)	3.154(7)
O1···H16^{iv}	2.214	2.132(6)	2.139(8)
O1···C7^{iv}	3.187(3)	3.1318(3)	3.118(7)
O1···H11^{i}	2.730	2.499(6)	2.457(7)
O1···C13^{i}	3.654(3)	3.5714(4)	3.545(7)
N1···H2^{i}	2.701	2.493(5)	2.473(8)
N1···C3^{i}	3.607(2)	3.5455(4)	3.522(9)
N1···H14^{ii}	2.696	2.519(6)	2.489(7)
N1···C14^{ii}	3.476(3)	3.4138(4)	3.394(6)
N1···H12^{ii}	2.890	2.822(6)	2.790(9)
N1···C13^{ii}	3.600(3)	3.5503(4)	3.528(8)
O1···O2^{ii}	4.324(2)	4.2655 (3)	4.243(9)
O1···O2^{i}	4.721(2)	4.6392 (3)	4.612(9)
H5···H13^{ii}	2.270	2.152(8)	2.14(1)

[a] (i) 1+*x*, *y*, *z*; (ii) 1/2−*x*, 1/2+*y*, 3/2−*z*; (iii) 1−*x*, −*y*, 2−*z*; (iv) 1/2+*x*, 1/2−*y*, *z*−1/2.

at very low temperature. A similar behavior was observed on 2-ethynyladamantan-2-ol.[55]

At 110 K, the two N−O bond distances differ significantly [N_2-O_1 = 1.2839(3) Å and N_3-O_2 = 1.2708(3) Å], and this difference also persists at room temperature[22] and at 6.5 K.[24] This disymmetry is also observed in other NN free radicals[9,41−45] or when the nitronyl forms a complex with copper(II) salts[45,56] (vide supra). From room temperature to 110 K, the twist of the pyridine ring around the C_5-C_8 bond decreases from 48.1° to 46.4°, but this variation does not lead to any particular effect (45.8° at 6.5 K).

TABLE 4b: Selected Bond Angles (degree) at 110 K at the End of the Multipolar Refinement

C5−N1−C1	116.75(2)	C7−C6−C1	177.62(5)
O1−N2−C8	125.90(2)	N2−C8−N3	109.34(2)
O1−N2−C9	121.81(2)	N2−C8−C5	124.54(2)
C8−N2−C9	111.90(2)	N3−C8−C5	125.90(2)
O2−N3−C8	126.66(2)	N2−C9−C12	109.72(2)
O2−N3−C10	121.32(2)	N2−C9−C11	106.98(2)
C8−N3−C10	110.90(2)	N2−C9−C10	100.64(2)
N1−C1−C2	123.31(2)	C12−C9−C11	110.09(2)
N1−C1−C6	116.81(2)	C12−C9−C10	114.90(2)
C2−C1−C6	119.88(2)	C11−C9−C10	113.79(2)
C3−C2−C1	118.77(2)	N3−C10−C3	109.82(2)
C2−C3−C4	118.61(2)	N3−C10−C14	105.04(2)
C3−C4−C5	118.43(2)	N3−C10−C9	101.16(2)
N1−C5−C4	124.12(2)	C13−C10−C14	110.55(2)
N1−C5−C8	117.35(2)	C13−C10−C9	115.51(2)
C4−C5−C8	118.51(2)	C14−C10−C9	113.76(2)
O2···H1^{iii}−C2^{iii}	129.5(2)	N1···H2^{i}−C3^{i}	162.9(2)
O2···H3^{i}−C4^{i}	123.1(2)	N1···H14^{ii}−C14^{ii}	138.1(3)
O1···H16^{iv}−C7^{iv}	156.3(3)	N1···H12^{ii}−C13^{ii}	124.0(2)
O1···H11^{i}−C13^{i}	170.1(3)		

(i) 1+*x*, *y*, *z*; (ii) 1/2−*x*, 1/2+*y*, 3/2−*z*; (iii) 1−*x*, −*y*, 2−*z*; (iv) 1/2+*x*, 1/2−*y*, *z*−1/2.

TABLE 5: Results of the Hirshfeld Rigid Bond Test

X−Y bond	*Z*(X) (Å^2)[a]	*Z*(Y) (Å^2)[a]	Δ*Z* (Å^2)[b]
Ethynyl Function			
C6−C7	0.0240	0.0336	0.0096
C1−C6	0.0179	0.0242	0.0063
Pyridine Ring			
N1−C5	0.0167	0.0161	−0.0006
N1−C1	0.0128	0.0132	0.0004
C1−C2	0.0177	0.0181	0.0004
C2−C3	0.0193	0.0196	0.0004
C3−C4	0.0164	0.0160	−0.0004
C4−C5	0.0162	0.0156	−0.0006
C5−C8	0.0129	0.0128	−0.0001
Nitronyl Ring			
N2−O1	0.0167	0.0160	−0.0007
N3−O2	0.0160	0.0166	0.0006
N2−C8	0.0133	0.0141	0.0008
N3−C8	0.0156	0.0160	0.0004
N2−C9	0.0155	0.0162	0.0007
N3−C10	0.0156	0.0157	0.0001
C9−C10	0.0210	0.0205	−0.0005
C9−C11	0.0181	0.0312	0.0131
C9−C12	0.0178	0.0340	0.0162
C10−C13	0.0159	0.0153	−0.0006
C10−C14	0.0158	0.0165	0.0007

[a] *Z*(X) and *Z*(Y) are the components of the thermal ellipsoids of atom X and Y along the bond direction. [b] Δ*Z* is the difference between *Z*(X) and *Z*(Y).

Rigid Bond Test and Atomic Displacement Amplitudes (ADP) Analysis. The Hirshfeld rigid bond test,[57] performed on X-ray and on neutron results (Table 5), shows large Δ*Z* values for some bonds involving a methyl group, on one side of the nitronile ring (C_9-C_{11}, C_9-C_{12}) and the ethynyl function. The less the methyl hydrogen atoms are involved in the network of intermolecular contacts, the more the vibration is important.

To get more information on internal motions, the thermal displacement tensors of the HC≡CPyNN radical were analyzed using the TLS[58] formalism. The **T**, **L**, and **S** matrix elements were refined using the least-squares program EKRT[59] against the observed atomic displacement parameters obtained at the end of the multipolar refinement. The agreement indices (R_w =

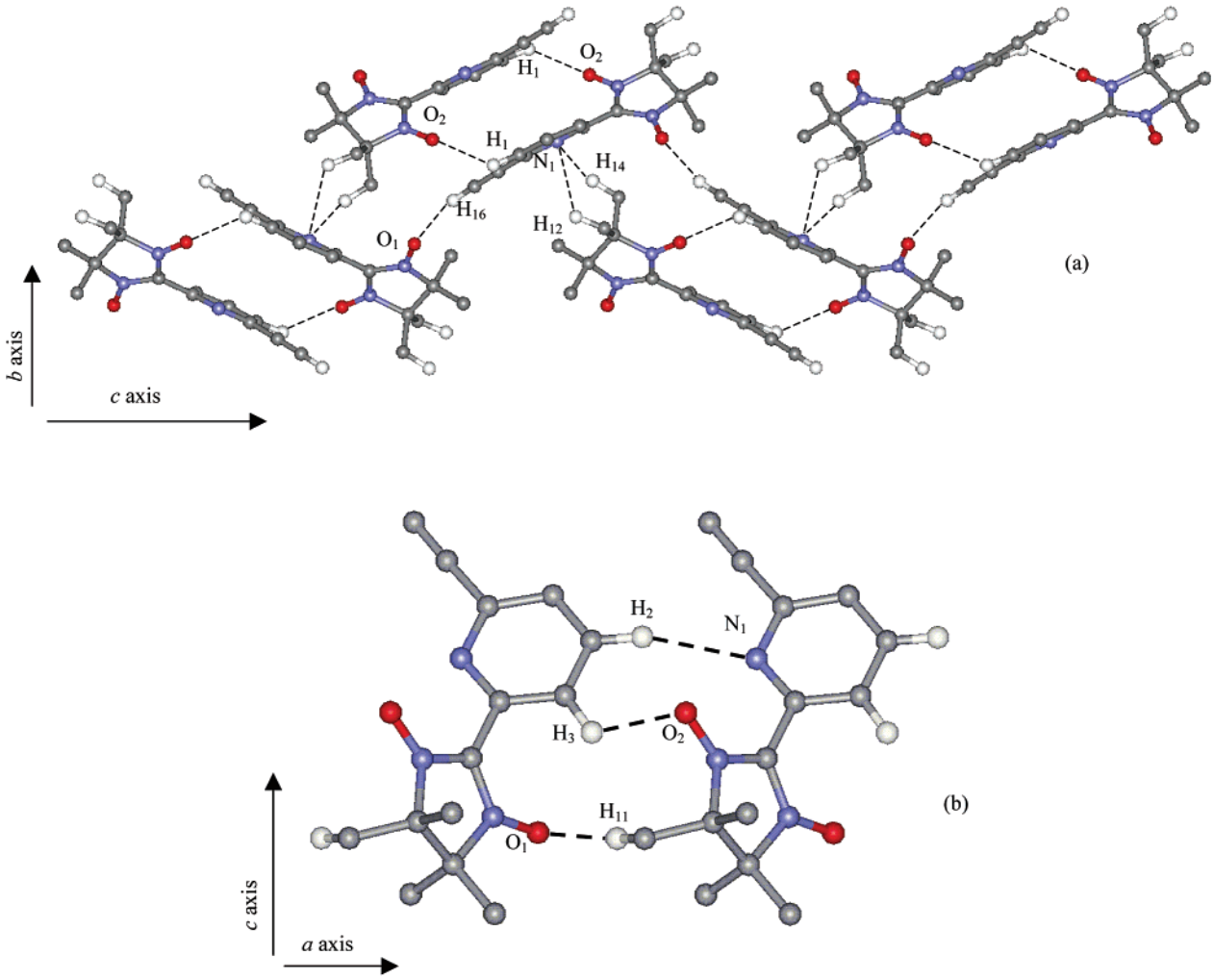

Figure 3. The crystal packing and intermolecular hydrogen bonds of HC≡CPyNN: (b) view along the *c* axis and (a) view along the *a* axis (only the H atoms involved in the close intermolecular interactions are represented).

11.3%, GOF = 20.4) are high for the rigid body model,[60] which means that HC≡CPyNN cannot be described as a rigid unit. Therefore, three chemical internal vibration modes were added in the TLS refinement. Two motions, τ_1 and τ_2, describe the vibration of the nitronyl ring (Figure 4): τ_1 represents the libration of C_9 to C_{14} atoms around the C_5-C_8 axis, and τ_2 is a vibration of the same atoms around the N_2-N_3 axis. In addition, an internal vibration, θ, was applied to the NN cycle and allowed bending around an axis perpendicular to the cycle passing through C_8 atom. The refinement of these internal vibrations reduced significantly the agreement indices (R_w = 7.8% and GOF = 14.4): large librations are observed around τ_1 and τ_2, which correspond to the vibration of the methyl groups (Table 6). The internal vibrations result in less extension of the oxygen atoms. It is worthy to underline that O_1, O_2, H_{11}, and H_{12}, (linked to C_{13}) and H_{14} (linked to C_{14}) are involved in intermolecular contacts. Comparing the thermal vibrations of these two methyl groups to the two other methyl groups (C_{11} and C_{12}), the latter are found to be 17% more agitated, which is consistent with the fact that the intermolecular contacts should reduce the ADPs of the atoms involved.

TABLE 6: TLS and Internal Motions[a]

T_{11} (Å^2)	T_{22}	T_{33}
0.0140(5)	0.0147(4)	0.0129(3)
L_{11} (°^{2})	L_{22}	L_{33}
1.7(0.2)	0.9(0.2)	7.2(0.6)
Internal Vibrations (°^{2})		
τ_1	12.5(2.4)	
τ_2	16.0(2.1)	
θ	6.7(1.3)	

	R_w[b]	GOF[c]
rigid body	0.113	20.6
full model	0.078	14.4

[a] ΔU^{ij} is the difference between "observed" and calculated ADPs, N_o is the number of observations (114), and N_p is the number of refined parameters (23). τ_i is a torsional angle, θ_i is a bending angle. T and L principal values are given with respect to the inertial principal axis of the molecule. The principal axis *Z* is nearly along C_5-C_8 bond. [b] $R_w = \{[\sum(\Delta U^{ij}/\sigma(U^{ij}))^2]/[\sum(U^{ij}/\sigma(U^{ij}))^2]\}^{1/2}$. [c] GOF = $\{[\sum(\Delta U^{ij}/\sigma(U^{ij}))^2]/[N_o - N_p]\}^{1/2}$.

Deformation Density and Topological Properties

The static deformation density maps (Figure 5) are drawn in two planes: the pyridine ring (5a) and the nitronyl ring (5b). For more quantitative discussion, Table 7 sums up topological properties at bond critical points (CP) involving non-H atoms in HC≡CPyNN, and Table 9 is devoted to topological and energetic properties of the intermolecular contacts.

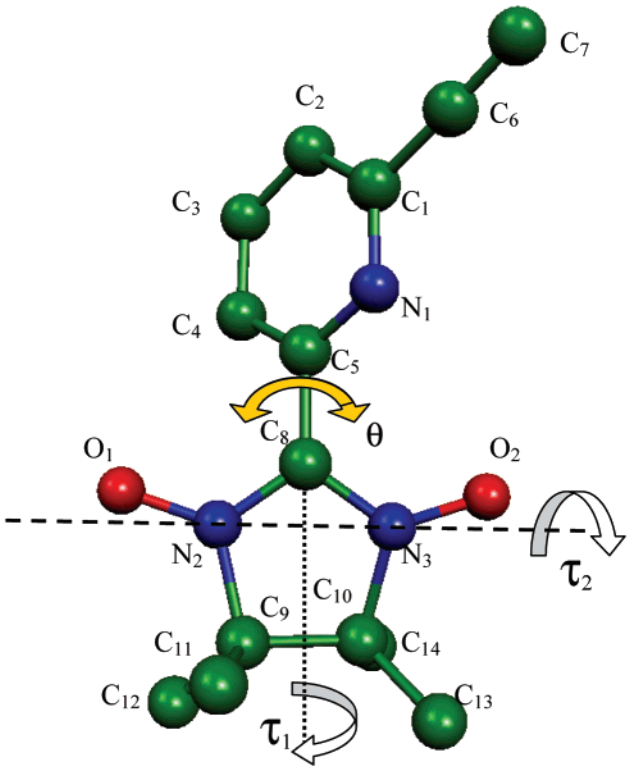

Figure 4. View and labeling of the internal vibrational modes. θ_i are in-plane bending and τ_i are torsional vibrations.

The Pyridine Ring and the Triple Bond. The experimental deformation density maps (Supporting Information Figure S2) show, as expected, a very high bonding density in the C_6-C_7 triple bond ($\Delta\rho$ = 0.65 eÅ^{-3}, d = 1.2061(3) Å), which is extended with approximate cylindrical symmetry in the plane perpendicular to the bond. The bonding densities around N1 ($\langle\Delta\rho\rangle$ = 0.38 eÅ^{-3}, $\langle d\rangle$ = 1.344 Å) are slightly lower than those observed for the C−C bonds in the pyridine ring ($\Delta\rho_{max}$ = 0.40 eÅ^{-3}, $\langle d\rangle$ = 1.396 Å) or for the bridging C_5-C_8 bond ($\Delta\rho$ = 0.45 eÅ^{-3}, d = 1.4706(3) Å), which has some double bond character. In agreement with the experimental deformation density, the static deformation density in the triple bond is high ($\Delta\rho$ = 0.80 eÅ^{-3}, Figure 5a). All C−C pyridine peaks are similar within the estimated standard deviation ($\langle\Delta\rho_{C-C}\rangle$ = 0.65 eÅ^{-3}) and close to the heights of the corresponding bonds in (*Z*)-*N*-acetyl-α,*β*-dehydrophenylalanine methylamide[61] or in the NNPhSMe radical[25] ($\langle\Delta\rho_{C-C}\rangle$ = 0.65 eÅ^{-3}). The bridging C_5-C_8 bond ($\Delta\rho$ = 0.64 eÅ^{-3}, d = 1.4706(3) Å) exhibits a deformation density close to that of the C−C pyridine bond ($\langle\Delta\rho_{max}\rangle$ = 0.66 eÅ^{-3}), different from that of a single C−C bond density (C_9-C_{10}: $\Delta\rho_{max}$= 0.48 eÅ^{-3}). The deformation density of the C_1-C_6 bond has an intermediate value ($\Delta\rho_{max}$ = 0.50 eÅ^{-3}).

The topological properties at the pyridine C−C bond critical points (CP) ($\langle\rho\rangle$ = 2.07 eÅ^{-3}, $\langle\nabla^2\rho\rangle$ = −21 eÅ^{-5}, $\langle\epsilon\rangle$ = 0.23) and at pyridine $C-N_1$ bond CPs ($\langle\rho\rangle$ = 2.27 eÅ^{-3}, $\langle\nabla^2\rho\rangle$ = −23 eÅ^{-5}, $\langle\epsilon\rangle$ = 0.17) are in agreement with those reported for similar bonds ($\langle\nabla^2\rho_{C-C}\rangle$ = −18.5 eÅ^{-5} and $\langle\nabla^2\rho_{C-N}\rangle$ = −18 eÅ^{-5} in average),[47,50−52] the Laplacian being slightly higher in our case. The characteristics of the two bridging bonds, C_5-C_8 and C_1-C_6, are similar (Table 7) and intermediate between a pyridine C−C bond and a pure single C−C bond, as a consequence of the electronic delocalization effects in HC≡CPyNN which increase electron density in the bonds involved in the delocalization pathway. As expected, compared to a pyridine C−C bond, the topological properties of triple C≡C bond are high density and large magnitude of $\nabla^2\rho$ at the CP, with a cylindrical symmetry (ϵ = 0.07).

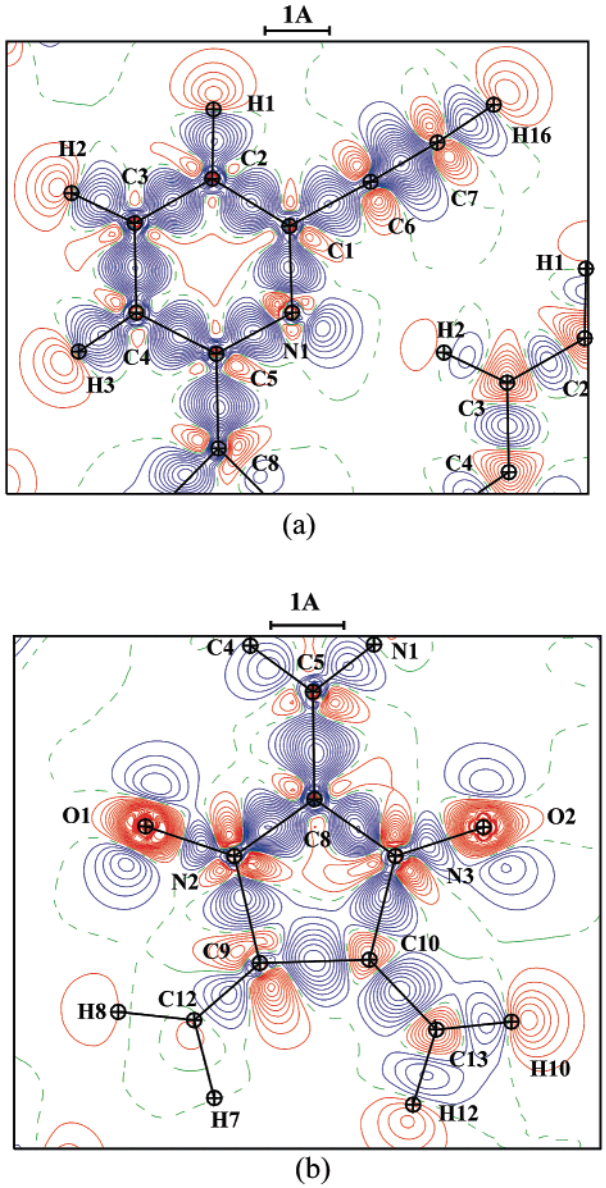

Figure 5. Static deformation density in (a) the pyridine ring and (b) the nitronyl ring plane. Contours of 0.05 eÅ^{-3} (positive contours in solid lines (red), negative contours in short dashed lines (blue), and long dashed lines for zero contour).

Nitronyl Nitroxide Ring. The deformation density and the topological properties of the two C−N ($\langle\Delta\rho_{max}\rangle$ = 0.65 eÅ^{-3}) and the two (N−O)• ($\langle\Delta\rho_{max}\rangle$ = 0.38 eÅ^{-3}) bonds of the nitronyl nitroxide group compare well within the accuracy of the experiment. The (N−O)• bond CP show a high electron density ($\langle\rho_{CP}\rangle$ = 2.74 eÅ^{-3}) associated to a very small positive Laplacian value ($\langle\nabla^2\rho_{CP}\rangle$ = 1.9 eÅ^{-5}) and a very large curvature along the bond ($\langle\lambda_3\rangle$ = 47 eÅ^{-5}). These values are in excellent agreement with our previous results on NNPhSMe[25] ($\langle\rho_{CP}\rangle$ = 2.68 eÅ^{-3}, $\langle\nabla^2\rho_{CP}\rangle$ = 4.9 eÅ^{-5}). By comparison, the corresponding characteristics for a "normal" N−O bond as in 1-phenyl-4-nitroimidazole[46] are $\langle\rho_{CP}\rangle$ = 3.15 eÅ^{-3}, $\langle\nabla^2\rho_{CP}\rangle$ = −3.6 eÅ^{-5}, and $\langle\lambda_3\rangle$ = 50 eÅ^{-5} for a shorter N−O distance ($\langle d_{N-O}\rangle$ = 1.227 Å). Similar values are also given by Zhurova and Pinkerton for energetic materials containing NO_2,[51] but smaller than what was observed for free NO_2 group ($\nabla^2\rho$ =

TABLE 7: Topological Properties at the Bond Critical Points

bond (X−Y)	d(X−Y) (Å)	dist. (X−Cp) (Å)	dist. (Y−Cp) (Å)	$\rho(\vec{r}_{cp})$ (eÅ^{-3})	$\rho-\rho_{pro}$ (eÅ^{-3})[a]	$\nabla^2\rho(\vec{r}_{cp})$ (eÅ^{-5})	ϵ	λ_3
C6−C7	1.206	0.574	0.632	2.76	0.87	−30	0.07	5.8
C6−C1	1.438	0.709	0.729	1.83	0.51	−15	0.08	9.2
C1−C2	1.402	0.711	0.694	2.02	0.62	−19	0.25	7.6
C2−C3	1.389	0.673	0.716	2.10	0.67	−22	0.19	6.7
C3−C4	1.391	0.692	0.699	2.14	0.71	−22	0.25	7.2
C4−C5	1.398	0.642	0.756	2.03	0.65	−19	0.21	7.2
C5−N1	1.340	0.549	0.793	2.26	0.56	−23	0.16	11
C1−N1	1.347	0.562	0.785	2.27	0.58	−23	0.18	11
C5−C8	1.471	0.678	0.792	1.85	0.64	−17	0.10	8.2
C8−N2	1.347	0.520	0.826	2.30	0.71	−23	0.20	12
C8−N3	1.356	0.528	0.828	2.22	0.61	−26	0.25	9.5
N2−O1	1.284	0.642	0.642	2.70	0.40	1.0	0.11	46
N3−O2	1.271	0.622	0.648	2.78	0.35	2.8	0.06	47
C9−N2	1.509	0.612	0.897	1.54	0.45	−8.2	0.09	10
C10−N3	1.506	0.617	0.889	1.65	0.55	−11	0.11	11
C9−C10	1.555	0.775	0.780	1.58	0.48	−12	0.07	8.0
C11−C9	1.533	0.730	0.802	1.59	0.47	−12	0.03	7.4
C12−C9	1.522	0.710	0.812	1.60	0.48	−12	0.03	7.5
C13−C10	1.521	0.715	0.806	1.58	0.45	−12	0.06	7.2
C14−C10	1.523	0.725	0.806	1.54	0.43	−11	0.06	7.2

[a] ρ_{pro} is the pro-molecule electron density (i.e., the sum of spherical independent atoms): (i) $1+x, y, z$; (ii) $1/2-x, 1/2+y, 3/2-z$; (iii) $1-x, -y, 2-z$; (iv) $1/2+x, 1/2-y, z-1/2$.

TABLE 8: Net Atomic Charges Obtained by Integration over Atomic Basins for HC≡CPyNN and NNPhSMe

	HC≡CPyNN		NNPhSMe	
name	Q_{int}	volume	Q_{int}	volume
O1	−0.36	17.59	−0.40	18.21
O2	−0.32	16.69	−0.35	17.31
N1	−1.00	13.99		
N2	−0.70	9.42	−0.35	8.66
N3	−0.52	9.46	−0.40	9.01
C8	0.59	8.15	0.58	7.56
C1	0.29	9.09	−0.04	10.31
C5	0.27	8.63	0.08	9.91
C2	−0.28	13.91	−0.59	14.60
C3	−0.34	13.59	−0.33	13.72
C4	−0.23	12.74	−0.27	13.67
			−0.41	13.47
C9	0.12	6.04	0.12	5.80
C10	0.16	5.95	0.17	5.75
C11	−0.47	13.42	−0.71	13.59
C12	−0.52	13.52	−0.63	13.26
C13	−0.41	12.65	−0.70	14.03
C14	−0.51	12.77	−0.69	13.66
C6	−0.35	16.78		
C7	−0.29	22.78		
H (Pyr)	0.34	4.86	0.42	4.76
H (CH_3)	0.29	5.91	0.33	5.84
H16	0.49	4.15		

HC≡CPyNN			NNPhSMe		
function	charge	volume	function	charge	volume
O−N−C−N−O	−1.31	61.31	O−N−C−N−O	−0.92	59.00
ethynyl	−0.15	43.72	S−CH_3	−0.47	62.32
pyridine	−0.26	86.53			

−43 eÅ^{-5}).[62] Consequently, adding an electron in the π^* antibonding molecular orbital has a great effect on the Laplacian value, which becomes positive. Therefore, according to the local Viriel theorem (in atomic units, eq 6),

$$\frac{1}{4}\nabla^2\rho(\vec{r}) = 2G(\vec{r}) + V(\vec{r}) \qquad (6)$$

with G and V being the kinetic and potential energy densities, respectively, the increase of the Laplacian value from −3.6 eÅ^{-5} to 1.9 eÅ^{-5} shows that the contribution of kinetic energy density is in excess at the (N−O)$^\bullet$ bond CP, and the charge density at CP is correspondingly depleted. This picture is characteristic of this type of covalent bond. It also explains why the density at CP is 15% smaller than that of a normal N−O covalent bond, while the corresponding bond length is only approximately 4% smaller.

On the contrary, the CP properties of the two nitronyl nitroxide C_8−N bonds are equal ($\langle\rho_{CP}\rangle$ = 2.26 eÅ^{-3}, $\langle\nabla^2\rho_{CP}\rangle$ = −24 eÅ^{-5}, $\langle\epsilon\rangle$ = 0.22) and similar to the pyridine C−N_1 bonds ($\langle\rho_{CP}\rangle$ = 2.26 eÅ^{-3}, $\langle\nabla^2\rho_{CP}\rangle$ = −23 eÅ^{-5}, $\langle\epsilon\rangle$ = 0.17) which show a mixed $\sigma-\pi$ character confirmed by its bond ellipticity. These bonds are clearly different from the two long C−N bonds (N_2−C_9 and N_3−C_{10}, $\langle d\rangle$ = 1.507 Å, $\langle\rho_{CP}\rangle$ = 1.60 eÅ^{-3}, $\langle\nabla^2\rho_{CP}\rangle$ = −9.4 eÅ^{-5}), for which topological properties correspond to single bonds such as C_9−C_{11}, C_9−C_{12}, C_{10}−C_{13}, or C_{10}−C_{14} (Table 7).

In conclusion, inspection of deformation density maps and of topological properties of the NN radical show that (i) the four C_1−C_6, C_5−C_8, C_8−N_2, and C_8−N_3 bonds share a common characteristic, a mixed $\pi-\sigma$ character due to the electron delocalization scheme from the ethynyl subunit to the two nitro-oxygen atoms. This phenomenon can be a partial explanation of the spin density on H_{16} evidenced by the PND experiment,[23] and (ii) the topological properties of the (N−O)$^\bullet$ bonds are clearly different from those of normal N−O. The antibonding electron leads to a larger bond length and lower density than in the normal N−O bond and to a positive Laplacian at the CP.

Net Atomic Charges. The atomic charges obtained by integration over on the atomic basins determined by (eq 7)

$$\vec{\nabla}\rho\cdot\vec{n} = 0 \qquad (7)$$

are given in Table 8 along with integrated charges for NNPhSMe.[63]

Both compounds have a large dipole moment, the positive charges being mainly shared by the Me_2−C_9−C_{10}−Me_2 groups, whereas the remaining part of the molecule is negatively charged with an exception corresponding to the C_8 atom (+0.59 e in HC≡CPyNN and +0.58 e in NNPhSMe). The whole conjugated part of each radical is therefore negatively charged.

The charge of the NN group in HC≡CPyNN (−1.31 e) is 0.41 e more negative than that of the corresponding group in NNPhSMe (−0.92 e). Conversely, the S−CH_3 group (−0.47 e) appears to be more negative than the ethynyl group (−0.15

TABLE 9: Topological and Energetic Properties of Intermolecular Contacts

bond (X−Y)[a]	*d*(X−Y) (Å)	*d*(X−Cp) (Å)	*d*(Y−Cp) (Å)	$\rho(\vec{r}_{cp})$ (eÅ^{-3})	$\nabla^2\rho(\vec{r}_{cp})$ (eÅ^{-5})	λ_3 (eÅ^{-3})	kinetic energy density[64] (KJ mol^{-1} per atomic unit volume)
O1···H16^{iv}	2.132	1.387	0.805	0.07	1.4	1.9	30
O1···H11^{i}	2.499	1.569	0.956	0.04	0.69	0.92	14
O2···H1^{iii}	2.309	1.382	0.992	0.09	1.1	1.8	26
O2···H3^{i}	2.457	1.432	1.095	0.07	0.87	1.3	20
N1···H2^{i}	2.493	1.581	0.926	0.05	0.85	1.1	18
N1···H14^{ii}	2.519	1.533	1.021	0.06	0.80	1.2	18
N1···H12^{ii}	2.822	1.668	1.172	0.05	0.54	0.68	12
H5···H13^{ii}	2.152	1.129	1.023	0.05	0.66	0.96	14

[a] (i) 1+*x*, *y*, *z*; (ii) 1/2−*x*, 1/2+*y*, 3/2−*z*; (iii) 1−*x*, −*y*, 2−*z*; (d) 1/2+*x*, 1/2−*y*, *z*−1/2.

e), the pyridine group being slightly negative (−0.27 e) due to the N_1 nitrogen atom, compared to the NNPhSMe phenyl group (+0.12 e). In HC≡CPyNN, the largest carbon atomic volumes are those of C_7 and C_6 atoms, 16.8 and 22.8 Å^3, respectively, compared to approximately 13 Å^3 for the C_2, C_3, or C_4 pyridine atoms which almost bear the same integrated charge (≈ −0.28 e). Therefore, the charge density of the C≡C triple bond expands over a very large volume, almost 40 Å^3, whereas H_{16}, being 0.49 e positively charged, has the most contracted (4.1 Å^3) volume.

The (N−O)$^\bullet$ oxygen atom's volumes and charges (17.1 Å^3, −0.34 e, Table 8) are slightly different from those of the corresponding oxygens of the NO_2 group of 1-phenyl-4-nitroimidazole[46] (17.3 Å^3 and −0.42 e). The difference in bonding lies in the nitrogen atom, which is positively charged in NO_2 (0.21 e for a volume of 8.2 Å^3), whereas in (N−O)$^\bullet$ the nitrogen atom has a negative charge equal (NNPhSMe) or even larger (this work) than the oxygen ones. This is related to the spin density observed in PND experiments.

As seen before, the pyridine ring negative charge is mainly due to the N_1 nitrogen atom, which also possesses a large volume (14.0 Å^3 and −1.0 e), compared to the nitroxide nitrogens (9.4 Å^3 and −0.53 e). The electro-attractive effect of N_1 also appears very clearly when one compares its charge and volume to those of the C_1 and C_5 carbon atoms to which it is bonded (8.8 Å^3 and +0.28 e).

Intermolecular Contacts. Both O_1 and O_2 atoms are involved in two intermolecular hydrogen bonds (HB): O_2 is linked to the pyridine ring of the two neighboring molecules (via H_1-C_2 and H_3-C_4), whereas O_1 is linked to the ethynyl group (via $H_{16}-C_7$) and to a methyl group (via $H_{11}-C_{13}$). The shortest bond $O_1\cdots H_{16}$ (d = 2.132(6) Å) has a large electrostatic character due to high charges of both O_1 and H_{16} (Table 8). This explains the smaller electron density (ρ_{CP} = 0.07 eÅ^{-3}) at the $O_1\cdots H_{16}$ CP, compared to $O_2\cdots H_1$ contact (ρ_{CP} = 0.09 eÅ^{-3}, d = 2.309(5) Å). This latter HB strengthens the centrosymmetric dimer (molecules (*x*, *y*, *z*) and (1−*x*, −*y*, 2−*z*)) which, as shown above, also exist in ITPyC≡CH, only stabilized by a $\pi-\pi$ interaction (no HB). This $\pi-\pi$ interaction contributes to increase the charge density at CP.

Due to its −1.0 e net charge, N_1 generates a large negative electrostatic potential which enables three weak HB with methyl and pyridine hydrogens.

Previous studies[22−24] have pointed out that the $O_1\cdots H_{16}-C_7$ contact leading to the zigzag chain is responsible for the ferromagnetic interaction at low temperature. As discussed above, the intermolecular contacts involve one molecule and its four neighbors and confer a three-dimensional character to the intermolecular interactions. To estimate the relative strength of these C−H···O and C−H···N hydrogen bonds, the kinetic energy density according to Abramov[64] ($G_{cp}(r)$ = $(3/10)(3\pi^2)^{2/3}\rho_{cp}(r)^{5/3} + (1/6)\nabla^2\rho_{cp}(r)$) was calculated (Table 9). As expected, the highest energy density is found in the $O_1\cdots H_{16}^{vi}$ contact (30 KJ mol^{-1} per atomic unit volume), followed by $O_2\cdots H_1^{iii}$ contact (26 KJ mol^{-1} per atomic unit volume). The other contacts have slightly lower energies. According to the first McConnell model[17] for $O_1\cdots H_{16}^{vi}$ or to the second McConnell model[18] for all C−H···O−N bonds, this network may induce ferromagnetic interactions.

Conclusion

This detailed analysis of the electron density gives complementary information that can be used, in parallel with the polarized neutron data, to explore the possible mechanisms governing the magnetic order in HC≡CPyNN.[24]

Concerning the NN function, many structural studies at room temperature have been carried out. Some of them are accurate enough to allow a comparison of the N−O and C−N distances.[9,41−45] For many compounds, a bond length alternation is observed: a short N−O bond alternating with a corresponding long C−N bond on one side and vice-versa on the other side. To have a global understanding of this phenomenon, which is also observed for HC≡CPyNN, a systematic study was carried out on all accurate NN structures stored in the CCDC.[54] The NN compounds found are split in three groups: (1) NN complexing one metallic center with one (N−O)$^\bullet$ group, (2) NN functioning as ligand between two metallic centers and (3) (N−O)$^\bullet$ not involved in specific bonds. In each case, bond length alternation is always predominant. In the first group, alternation is induced by the interaction with the metallic center, so the differences between the two N−O or C−N bond lengths or alternation frequency (five alternating for one non alternating, Table 10) are larger than in other groups. When we consider the third group (no metal coordination), alternation is present in approximately 60% of the compounds. However, when the (R) group linked to NN is symmetric (no intramolecular effects), alternation is also observed (frequency 74% and amplitude (0.011(6) Å for N−O and 0.014(5) Å for C−N, Table 10). Therefore, this alternation is a consequence of the relative strength of the intermolecular interactions involving the two oxygen atoms of the NN function. As shown above from the topological analysis, the small positive Laplacian value at the (N−O)$^\bullet$ CP, corresponding to electron depletion at CP and charge accumulation at the nuclei, favors intermolecular interactions via charge transfer.

The study of the topological properties of all bonds reveals the electron delocalization from the ethynyl function to the nitronyl nitroxide through the pyridine ring. All bonds possess a mixed $\sigma-\pi$ character, as observed in NNPhSMe. If the methyl groups mainly carry the positive net charges, the negative charge is mainly located on the nitronyl nitroxide function (−1.31 e), on the pyridine ring (−0.26 e) and on the ethynyl function

TABLE 10: Frequency and Amplitude of Bond Alternation of the NN Group

	⟨N−O⟩ 1[a] (Å)	⟨C−N⟩ 1[a] (Å)	⟨C−N⟩ 2[a] (Å)	⟨N−O⟩ 2[a] (Å)	no. of alternating cases	no. of nonalternating cases	total no. of cases
group I[b]	1.271(1)	1.353(1)	1.331(2)	1.295(2)	100	18	121
group II	1.280(3)	1.351(4)	1.340(3)	1.302(4)	20	10	34
group III	1.271(1)	1.352(2)	1.344(2)	1.286(2)	116	62	198
group III with symmetrical R	1.276(3)	1.357(3)	1.343(2)	1.287(3)	46	16	67
HC≡CpyNN	1.2708(3)	1.3559(3)	1.3466(3)	1.2839(3)			

[a] Labels 1 and 2 refer to short and long N−O distances, respectively. [b] For group I, the (C−N−O) group number 2 is linked to the metal. For group II, each (C−N−O) group is linked to a metal.

(−0.15 e). This delocalization scheme, coupled with the intermolecular $O_1 \cdots H_{16}$ contact, can explain the presence of spin density on H_{16} as observed on PND experiment. Moreover, this partial charge transfer is from the single occupied molecular orbital (SOMO), π^*, to the lower unoccupied molecular orbital (LUMO), mainly located on the pyridine group.[24] According to the second McConnell model,[18] this reinforces the ferromagnetic interaction along the short intermolecular hydrogen bond (2.132(6) Å) that links O_1 (SOMO) and H_{16} (LUMO), and also the predominance of ferromagnetic interactions above T_N (0.54 K).

A three-dimensional network of weak C−H···O and C−H···N hydrogen bonds links one molecule to four neighbors. As seen above, all bonds with partial π character are elongated when the temperature decreases; correlatively, the intermolecular contacts are significantly shortened. Therefore, the hydrogen bond network plays a more predominant role with decreasing temperature, increasing the ferromagnetic coupling at very low temperature and the charge density in the intermolecular region.

At 0.54 K the compound undergoes an antiferromagnetic transition. As all previously described intermolecular contacts induce ferromagnetic coupling, the explanation of that transition lies elsewhere. A possible explanation can be found considering the N−O···O−N interaction. As described in the packing section, the shortest distance between O_1 and O_2 atoms is 4.2655(3) Å (O_2: $(1/2)-x$, $(1/2)+y$, $(3/2)-z$), with quasi-perpendicular nitronyl nitroxide mean planes. Another short distance is observed between O_1 and O_2 ($1+x$, y, z) in the $\vec{a}$ direction (4.6392(3) Å). It is worthy to remember that this last one is particularly shortened with decreasing temperature. The first McConnell model predicts an antiferromagnetic coupling for this kind of contact: if these distances appear to be quite long for intermolecular contacts, they however are among the shortest observed by Deumal et al.[21] in their review of the nitronyl nitroxide family. Moreover, as each oxygen atom carries an important positive spin density, these interactions can explain the weak antiferromagnetic contribution appearing at very low temperature.

Acknowledgment. This research was supported by the Centre National de la Recherche Scientifique and the Université Henri Poincaré, Nancy I. N.C. is grateful to the Ministère de l'Education Nationale for a doctoral fellowship. N.C. expresses gratitude to Dr. S. Pillet for helpful discussion and for providing as with the data on NNPhSMe. F.R. and R.Z. thank the Engineering School of Chemistry in Strasbourg.

Supporting Information Available: Tables of atomic positions and displacement parameters; figures showing gradient trajectories, Laplacians, and experimental deformation density; CIF data. This material is available free of charge via the Internet at http://pubs.acs.org.

References and Notes

(1) (a) Kahn, O. *Molecular Magnetism*; VCH: New York, 1993. (b) *Molecular Magnetism: From Molecular Assemblies to the Devices*; Coronado, E., Delhaès, P., Gatteschi, D., Miller, J. S., Eds.; NATO ASI Series E 321; Kluwer Academic Publishers: Dordrecht, 1996.

(2) *Magnetism: Molecules to Materials. Models and Experiments*; Miller, J. S., Drillon, M., Eds.; Wiley-VCH: Weinheim, Germany, 2001.

(3) Polyhedron 2001, 20 congress San Antonio (VIIth International Conference on Molecular-based Magnets (ICMM 2000), San Antonio, TX, 16−21 September 2000); *Polyhedron* **2001**, *20*, 1305−1309.

(4) (a) Keana, J. F. W. *Chem. Rev*. **1978**, *78*, 37. (b) Caneschi, A.; Gatteschi, D.; Sessoli, R.; Rey, P. *Acc. Chem. Res.* **1989**, *22*, 392. (b) Caneschi, A.; Gatteschi, D.; Rey, P. *Prog. Inorg. Chem.* **1991**, *39*, 331.

(5) Kinoshita, M.; Turek, P.; Tamura, M.; Nozawa, K.; Shiomi, D.; Nakazawa, Y.; Ishikawa, M.; Takahashi, M.; Awaga, K.; Inabe, T.; Maruyama, Y. *Chem. Lett.* **1991**, 1225.

(6) (a) Osiecky, J. H.; Ullman, E. F. *J. Am. Chem. Soc*. **1968**, *90*, 1078. (b) Ullman, E. F.; Osiecky, J. H.; Boocock, D. G. B.; Darcy, R. *J. Am. Chem. Soc.* **1972**, *94*, 7049. (c) Awaga, K.; Inabe, T.; Okayama, T.; Maruyama, Y. *Mol. Cryst. Liq. Cryst*. **1993**, *232*, 79. (d) Ziessel, R. *Synthesis* **1999**, *1839*, Ulrich, G.; Stroh, C.; Ziessel, R. *C. R. Acad. Sci*. **2001**, *4*, 113.

(7) (a) Awaga, K.; Inabe, T.; Maruyama, Y. *Chem. Phys. Lett*. **1992**, *190*, 349. (b) Luneau, D.; Risoan, G.; Rey, P.; Grand, A.; Caneschi, A.; Gatteschi, D.; Laugier, J. *Inorg. Chem.* **1993**, *32*, 5616. (b) Luneau, D.; Romero, F. M.; Ziessel, R. *Inorg. Chem.* **1998**, *37*, 5078−5087. (c) Fegy, K.; Luneau, D.; Ohm, T.; Paulsen, C.; Rey, P. *Angew. Chem., Int. Ed.* **1998**, *37*, 1270. (d) Fegy, K.; Luneau, D.; Belorizky, E.; Novak, M.; Tholence, J.-L.; Paulsen, C.; Ohm, T.; Rey, P. *Inorg. Chem.* **1998**, *37*, 4524.

(8) (a) Awaga, K.; Inabe, T.; Maruyama, Y.; Nakamura, T.; Matsumoto, M. *Chem. Phys. Lett*. **1992**, *195*, 21. (b) Stumpf, H. O.; Ouahab, L.; Pei, Y.; Grandjean, D.; Kahn, O. *Science* **1993**, *261*, 447. (c) Inoue, K.; Iwamura, H. *J. Am. Chem. Soc*. **1994**, *116*, 3173. (d) Mitsunori, T.; Inoue, K.; Koga, N.; Iwamura, H. *J. Am. Chem. Soc.* **1995**, *117*, 2467. (e) Iwamura, H.; Inoue, K.; Hayamizu, T. *Pure Appl. Chem.* **1996**, *68*, 243. (f) Sugano, T.; Tamura, M.; Kinoshita, M.; Sakai, Y.; Ohashi, Y. *Chem. Phys. Lett*. **1992**, *200*, 235.

(9) Turek, P.; Nozawa, K.; Shiomi, D.; Awaga, K.; Inabe, T.; Maruyama, Y.; Kinoshita, M. *Chem. Phys. Lett*. **1991**, *180*, 327.

(10) Hosokoshi, Y.; Tamura, M.; Kinoshita, M. *Mol. Cryst. Liq. Cryst*. **1993**, *232*, 45.

(11) Awaga, K.; Maruyama, Y. *Chem. Phys. Lett*. **1989**, *158*, 556.

(12) Awaga, K.; Inabe, T.; Nagashima, U.; Maruyama, Y. *J. Chem. Soc., Chem. Commun*. **1989**, 1617.

(13) Veciana, J.; Cirujeda, J.; Rovira, C.; Vidal-Gancedo, J. *Adv. Mater*. **1995**, *7*(2), 221.

(14) Cirujeda, J.; Hernandez-Gasio, E.; Rovira, C.; Stanger, J. L.; Turek, P.; Veciana, J. *J. Mater. Chem*. **1995**, *5*(2), 243.

(15) Matsushita, M. M.; Izuoka, A.; Sugawara, T.; Kobayashi, T.; Wada, N.; Takeda, N.; Ishikawa, M. *J. Am. Chem. Soc*. **1997**, *119*, 4369.

(16) Awaga, K.; Sugano, T.; Kinoshita, M. *Chem. Phys. Lett*. **1987**, *141*, 540.

(17) McConnell, H. M. *J. Phys. Chem*. **1963**, *39*, 1910.

(18) McConnell, H. M. *Proc. R. A. Welch Found. Conf. Chem. Res*. **1967**, *11*, 144.

(19) Kahn, O.; Briat, B. *J. Chem. Soc., Faraday Trans*. **1976**, *72*, 268 and 1441.

(20) Novoa, J. J.; Deumal, M.; Veciana, J. *Synth. Met.* **1999**, *103*, 2283.

(21) Deumal, M.; Cirujeda, J.; Veciana, J.; Novoa, J. J. *Chem. Eur. J.* **1999**, *5*, 1631.

(22) Romero, F. M.; Ziessel, R.; De Cian, A.; Fischer, J.; Turek, P. *New J. Chem*. **1996**, *20*(9), 919.

(23) Pontillon, Y.; Ressouche, E.; Romero, F. M.; Schweizer, J.; Ziessel, R. *Physica B* **1997**, *234*−*236*, 788.

(24) Romero, F. M.; Ziessel, R.; Bonnet, M.; Pontillon, Y.; Ressouche, E.; Schweizer, J.; Delley, B.; Grand, A.; Paulsen, C. *J. Am. Chem. Soc*. **2000**, *122*, 1298.

(25) Pillet, S.; Souhassou, M.; Pontillon, Y.; Caneschi, A.; Gatteschi, D.; Lecomte, C. *New J. Chem.* **2001**, *25*, 131.

(26) Otwinowski, Z.; Minor, W. In *Methods in Enzymology, Vol. 276, Macromolecular Crystallography*, part A; Carter, C. W., Jr., Sweet, R. M., Eds.; Academic Press: New York, 1996; p 307.

(27) DeTitta, G. T. *J. Appl. Crystallogr*. **1985**, *18*, 75.

(28) Blessing, R. H. *J. Appl. Crystallogr*. **1989**, *22*, 396.

(29) Brown, P. J.; Mattheman, J. C. *The Cambridge Crystallographic Subroutine Library*, RL-81-063.

(30) Sheldrick, G. M. *Acta Crystallogr*. **1990**, *A46*, 467.

(31) Sheldrick, G. M. *SHELXL97*; University of Göttingen: Göttingen, Germany, 1997.

(32) Hansen, N. K.; Coppens, P. *Acta Crystallogr*. **1978**, *A34*, 909.

(33) Johnson, C. K. ORTEP II. Report ORNL-5738. Oak Ridge National Laboratory, Tennessee, 1976.

(34) Clementi, E.; Raimondi, D. L. *J. Chem. Phys*. **1963**, *41*, 2686.

(35) Stewart, R. F.; Davidson, E. R.; Simpson, W. T. *J. Chem. Phys*. **1965**, *43*, 175.

(36) Cromer, D. T. In *International Tables for X-ray Crystallography*; Ibers, J. A., Hamilton, W. E., Eds.; Kynoch Press: Birmingham; Vol. 148.

(37) Bader, R. F. W. *Atoms in molecules: a quantum theory*; The International Series Monographs in Chemistry; Clarendon Press: Oxford, 1990.

(38) Souhassou, M.; Blessing, R. H. *J. Appl. Crystallogr.* **1999**, *32*, 210.

(39) Pérès, N.; Boukhris, A.; Souhassou, M.; Gavoille, G.; Lecomte, C. *Acta Crystallogr*. **1999**, *A55*, 1038.

(40) Coppens, P.; Guru Row, T. N.; Leung, P.; Stevens, E. D.; Becker, P. J.; Yang, Y. W. *Acta Crystallogr*. **1979**, *A35*, 63.

(41) Sugawara, T.; Matsushita, M. M.; Izuoka, A.; Wada, N.; Takeda, N.; Ishikawa, M. *J. Chem. Soc., Chem. Commun.* **1994**, 1723.

(42) Hernàndez, E.; Mas, M.; Molins, E.; Rovira, C.; Veciana, J. *Angew. Chem., Int. Ed. Engl.* **1993**, *32*(6), 882.

(43) Rancurel, C.; Sutter, J.-P.; Le Hoerff, T.; Ouahab, L.; Kahn, O. *New J. Chem*. **1999**, 1333.

(44) Zheludev, A.; Barone, V.; Bonnet, M.; Delley, B.; Grand, A.; Ressouche, E.; Ray, P.; Subra, R.; Schweizer, J. *J. Am. Chem. Soc*. **1994**, *116*, 2019.

(45) Caneschi, A.; David, L.; Ferraro, F.; Gatteschi, D.; Fabretti, A. C. *Inorg. Chim. Acta* **1994**, *217*, 7.

(46) Kubicki, M.; Borowiak, T.; Dutkiewicz, G.; Souhassou, M.; Jelsch, C.; Lecomte, C. *J. Phys. Chem. B* **2002**, *106*, 3706.

(47) Bodar-Houillon, F.; Elissami, Y.; Marsura, A.; Ghermani, N. E.; Espinosa, E.; Bouhmaida, N.; Thalal, A. *Eur. J. Org. Chem.* **1999**, 1427.

(48) Bianchi, R.; Gatti, C.; Adovasio, V.; Nardelli, M. *Acta Crystallogr*. **1996**, *B52*, 471.

(49) Guillot, B.; Jelsch, C.; Lecomte, C.; in preparation.

(50) Yang, W.; Craven, B. M. *Acta Crystallogr*. **1998**, *B54*, 912.

(51) Zhurova, E.; Pinkerton, A. A. *Acta Crystallogr*. **2001**, *B57*, 359.

(52) Romero, F. M.; Ziessel, R.; Drillon, M.; Tholence, J.-L.; Paulsen, C.; Kyritsakas, N.; Fisher, J. *Adv. Mater.* **1996**, *8*(10), 826.

(53) Janiak, C. *J. Chem. Soc., Dalton Trans.* **2000**, 3885.

(54) Allen, F. H.; Bellard, S.; Brice, M. D.; Cartwright, B. A.; Doubleday, A.; Higgs, H.; Hummelink, T.; Hummelink-Peters, B. G.; Kennard, O.; Motherwell, W. D. S.; Rodgers, J. R.; Watson, D. G. *Acta Crystallogr*. **1979**, *B 35*, 2331.

(55) Allen, F. H.; Howard, J. A. K.; Hoy, V. J.; Desiraju, G. R.; Reddy, D. S.; Wilson, C. C. *J. Am. Chem. Soc*. **1996**, *118*, 4081.

(56) Caneschi, A.; Ferraro, F.; Gatteschi, D.; Ray, P.; Sessoli, R. *Inorg. Chem.* **1990**, *29*, 1756.

(57) Hirshfeld, F. L. *Acta Crystallogr*. **1976**, *A32*, 239.

(58) Willis, B. T. M.; Pryor, A. W. *Thermal Vibrations in Crystallography*; Cambridge University Press: Cambridge, 1975.

(59) He, X. M.; Craven, B. M. *Acta Crystallogr*. **1993**, *A49*, 10.

(60) Schomaker, V.; Trueblood, K. N. *Acta Crystallogr*. **1968**, *B24*, 63.

(61) Souhassou, M.; Ghermani, N. E.; Lecomte, C.; Rhomer, M. M.; Wiest, R.; Benard, M.; Blessing, R. H. *J. Am. Chem. Soc*. **1992**, *114*, 2371.

(62) Panek, J.; Latajka, Z. *Chem. Phys. Lett*. **2000**, *332*, 617.

(63) Pillet, S. Ph.D. Thesis, Université Henri Poincaré, Nancy I, France, 2001.

(64) Abramov, Y. *Acta Crystallogr*. **1997**, *A53*, 264.